

A review and discussion on laboratory investigations involving supercritical CO₂ for storage

Mahsan Basafa, Omid Mohammadzadeh, Lesley Anne James*

Department of Process Engineering, Faculty of Engineering and Applied Science, Memorial University of Newfoundland, St. John's, NL A1C 5S7, Canada

Abstract. The race is on towards net zero carbon emissions, and upstream research and service laboratories are quickly shifting from enhanced oil recovery laboratory analyses to CO₂ injection for storage. For the storage purpose, CO₂ is usually injected into geological formations (i.e., saline aquifers and depleted oil and gas reservoirs) as a dense supercritical fluid (Temperature > 31°C, Pressure > 7.38 MPa). The goal of this paper is to review some supercritical concepts and theory regarding CO₂ injection and storage, and to highlight laboratory and instrumentation considerations when working with supercritical CO₂. Once CO₂ dissolves into brine, carbonic acid forms which can interact with various minerals of the host rock, resulting in porosity and permeability changes. Therefore, geological CO₂ storage requires understanding of multiphase flow behaviour in porous media to evaluate CO₂ injectivity and transport, CO₂ residual trapping, and the risk of CO₂ leakage. The geochemical reactions occurring during CO₂ injection can alter rock pore structure, which further impacts capillary pressure and wetting and non-wetting phase relative permeabilities. This paper will review and discuss pertinent phase behaviour, mass transfer, fluid-fluid and fluid-rock interactions associated with CO₂ injection into saline aquifers and waterflooded depleted oil formations as principal targets for geological carbon storage. Depending on mineral composition, temperature, pressure, flow regime, brine composition, multiphase flow of CO₂ and water, and initial pore structure, some minerals may dissolve due to the formation of carbonic acid and pH reduction. We highlight challenges in working with supercritical CO₂, with liquid-like density and gas-like viscosity, compared to CO₂ gas such as measuring pH at *in-situ* conditions. Stability of clay and carbonate minerals in deep saline formations is strongly affected by pH changes in this region. Usually, pH of the brine samples taken from coreflooding setups during the course of CO₂ injection is measured at ambient conditions. However, once brine samples are brought to low-pressure conditions, CO₂ is released leading to an increase in pH, which is not representative of the high-pressure high-temperature *in-situ* conditions. Knowing that pH is important to understand chemistry of the subsurface fluids in the context of geological carbon storage, we review laboratory practices and suggest analytical methods. Considering various factors of rock mineralogy, sub-core heterogeneity, and wettability is crucial for optimizing CO₂ storage and ensuring the long-term success of geological carbon sequestration.

Keywords: CO₂ storage, supercritical CO₂, multiphase flow behaviour, pH measurement, analytical methods.

* Corresponding author: ljames@mun.ca

1 Introduction

Carbon dioxide is a greenhouse gas that causes global warming and climate change. To decrease the amount of CO₂ in the atmosphere, one method is to capture it from industrial processes and store it in geological formations safely and effectively. It is essential to comprehend the CO₂ behaviour in geological formations to guarantee that the storage is successful, and that the CO₂ is securely and permanently trapped underground.

The preferred geological formations for CO₂ storage are depleted oil and gas reservoirs and saline aquifers due to their large storage capacity [1, 2]. Deep saline aquifers, in particular, are considered the best option because they have great storage potential and are unlikely to cause negative environmental impacts [3]. However, there are potential drawbacks associated with CO₂ storage in saline aquifers such as the need to build infrastructure from scratch and the possibility of aquifer over-pressurization [4]. There is also limited data on the long-term behaviour of CO₂ in these formations, as well as overall lack of characterization data when compared with depleted oil and gas reservoirs, which underscores the importance of characterization, monitoring and verification programs for the current and future CO₂ storage projects.

Typically, CO₂ is injected into geological formations as a supercritical fluid. However, dynamic pressure-temperature conditions and changes in the brine salinity can cause CO₂ phase change. Thus, it is necessary to investigate the behaviour of other CO₂ phases (gas and dense liquid for instance) in the context of geological storage. To understand the CO₂ trapping mechanisms involved in subsurface formations, it is important to have a fundamental understanding of the physical chemistry of CO₂-brine-rock systems, which is the typical rock-fluid system found in aquifers and oil reservoirs [3, 5-7]. Critical physicochemical parameters include solution pH, which controls mineral stability and caprock integrity, as well as reactions rate(s) and equilibrium state of the reservoir rocks, that significantly affect changes in the formation's porosity and permeability [8, 9]. Ultimately, these factors determine the total CO₂ storage capacity, via different trapping mechanisms (as described below), and injectivity at a given site.

This article presents a thorough explanation of the principles involved in the injection and storage of carbon dioxide in geological formations, with the focus on saline aquifers and depleted oil and gas reservoirs. In this article, we examine the behaviour of carbon dioxide in various geological conditions as well as its interactions with the host rock, formation brine, and residual oil. Additionally, it provides an overview of laboratory and

instrumentation considerations when dealing with supercritical carbon dioxide, including the effects of multiphase flow in porous media and geochemical reactions. We also emphasize the importance of *in-situ* pH measurement as a crucial indicator in exploring the physical and chemical characteristics of CO₂-brine-rock systems at typical storage conditions.

2 CO₂ phase behaviour and its interactions with fluids

CO₂ injection into deep saline aquifers creates a complex system involving geomechanics, geochemistry, and non-isothermal effects. The properties of this system depend on the rock properties, fluids involved, and temperature and pressure conditions [10]. The fate of CO₂ is controlled by fluid dynamics, dissolution into brine, and mineral formation due to chemical reactions. These reactions can alter the rock pore structure and affect capillary pressure and relative permeabilities of different phases.

CO₂ can be injected into the geological formations as supercritical dense phase, dissolved in brine (i.e., carbonated waterflooding), or in the form of dense liquid phase [6, 11-13]. CO₂ is a supercritical fluid at pressures above 7.38 MPa and temperatures above 31°C (Fig. 1). In its supercritical state, CO₂ has a liquid-like density but gas-like viscosity. In the case of CO₂ injection into saline aquifers, the target depth for CO₂ storage must be greater than 800 m, so that CO₂ will be in the supercritical state. This has an operational advantage for CO₂ storage as more volumes of CO₂ can be stored per unit pore volume.

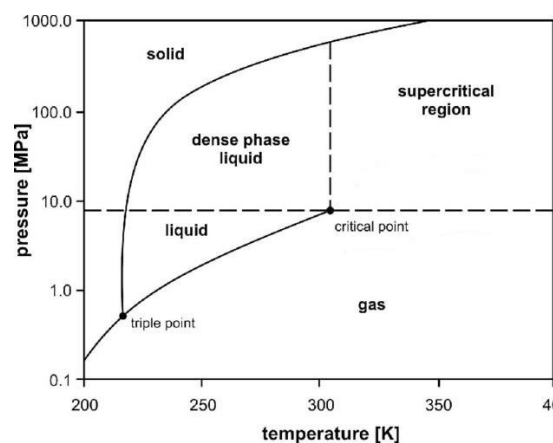


Fig. 1. CO₂ phase diagram [14]

Dissolution of CO₂ into the brine phase leads to a system of geochemical reactions which provide important characteristics for evaluation of CO₂ storage in saline aquifers. The overall transport process involves convective mixing and molecular diffusion of CO₂ through saline aqueous phase,

reactions with the host minerals, and convective mixing at the CO₂-brine interface that dominates the rate of CO₂ dissolution [15]. CO₂ solubility in brine increases with pressure and decreases with temperature and salinity [16, 17]. The effects of pressure and temperature on pH of a reservoir brine sample, saturated with CO₂, as well as CO₂ solubility in brine are shown in Fig. 2 and Fig. 3, respectively. The maximum CO₂ solubility in a synthetic brine (5.5 wt.% NaCl, 2.0 wt.% KCl, 0.45 wt.% MgCl₂, and 0.55 wt.% CaCl₂) at 40°C and 30 MPa was reported to be less than 1.2 mol/kg [16].

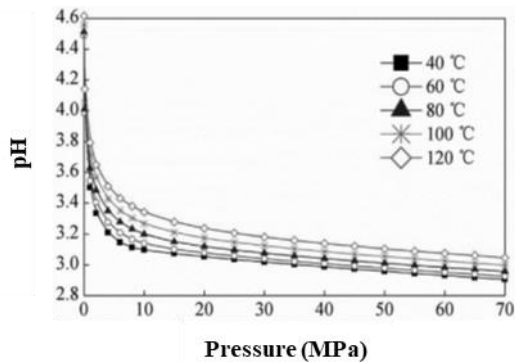


Fig. 2. pH of a synthetic brine sample (5.5% NaCl, 2.0% KCl, 0.45% MgCl₂, and 0.55% CaCl₂) saturated with CO₂ as a function of temperature and pressure, simulated using PHREEQC software [16]

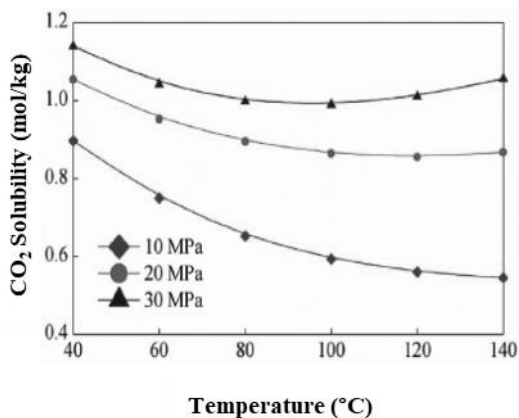


Fig. 3. CO₂ solubility in a synthetic brine sample (5.5% NaCl, 2.0% KCl, 0.45% MgCl₂, and 0.55% CaCl₂) as a function of temperature and pressure [16]

During CO₂ injection into saline aquifers, the CO₂ plume displaces brine at the pore-scale along with some CO₂ dissolution in brine, and the brine phase also dissolves into CO₂. The mass transfer of water into CO₂ is similar to evaporation of water and is also known as dry-out phenomenon. Dry-out increases salinity, leading to salt precipitation in the pore system [18, 19]. This can potentially result in pore blockage and permeability impairment, which can in turn affect CO₂ storage efficiency. Therefore, studying the phase behaviour of CO₂-water system at the storage condition is an important step in

evaluation of CO₂ injection for storage. Various methods have been used to determine water solubility in CO₂, and thermodynamic models have been developed for water-CO₂ phase equilibrium [20-24]. Wang et al. used *in-situ* quantitative Raman spectroscopy to measure water solubility in supercritical CO₂ at temperature and pressure ranges of 313.15 – 473.15 K (40 – 200°C) and 10 – 50 MPa, respectively, and improved the water solubility models using these measurements [25]. It was concluded that increasing the temperature causes an exponential increase in solubility of water in supercritical CO₂, whereas a more complex relationship exists between pressure and water solubility in CO₂ (Fig. 4).

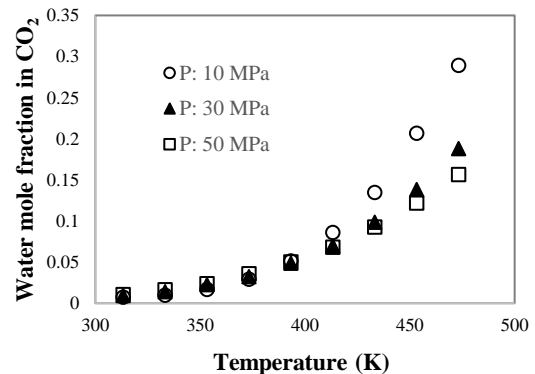


Fig. 4. Water solubility in CO₂ [25]

Another target storage site for CO₂ is depleted oil and gas reservoirs. In the case of CO₂ storage in waterflooded oil layers, some flow assurance challenges could arise when injected CO₂ is brought in contact with waterflood residual oil [26-29]. At higher injection pressures associated with supercritical CO₂ sequestration, increased CO₂ solubility in waterflood residual oil may trigger asphaltene destabilization and precipitation, which could result in permeability impairment depending on flow dynamic conditions, asphaltene content of the *in-situ* oil, temperature and pressure. In addition, the interfacial behaviour of hydrocarbon-brine systems is also influenced by the amount of dissolved CO₂ [30, 31].

In order to assess the performance of any CO₂ storage project, it is required to fully characterize the fluid pair systems containing CO₂. These include CO₂-brine as well as CO₂-oil fluid systems. Phase behaviour of CO₂-crude oil and CO₂-gas mixtures have been extensively studied in enhanced oil recovery (EOR) studies and can be used for understanding the behaviour of CO₂ in the presence of organic compounds for CO₂ storage in depleted oil and gas reservoirs [3, 32-34]. For the CO₂-oil fluid system, diffusion of CO₂ in oil reduces oil viscosity and density. The effective diffusion coefficient of supercritical CO₂ in *n*-decane in Berea core samples (50 and 100 mD permeabilities) was

determined at high pressure and high temperature (HPHT) conditions of 10 – 25 MPa and 333.15 – 373.15k (60 – 100°C), respectively [35]. The diffusion coefficient of supercritical CO₂ in oil increases with pressure, temperature, and permeability, and the effect of pressure on the diffusion process becomes less important at elevated temperatures. Furthermore, it was shown that the CO₂ diffusion in the bulk oil phase (i.e., *n*-decane) is impeded in the presence of porous media [35].

Mosavat and Torabi [12] measured CO₂ solubility in light crude oil using a high-pressure see-through-windowed cell (Fig. 5). Initial and final volumes of CO₂ were determined at various temperatures and pressures by taking photos from the cell, and the amount of CO₂ dissolved in oil was calculated using mass balance and ideal gas equations.

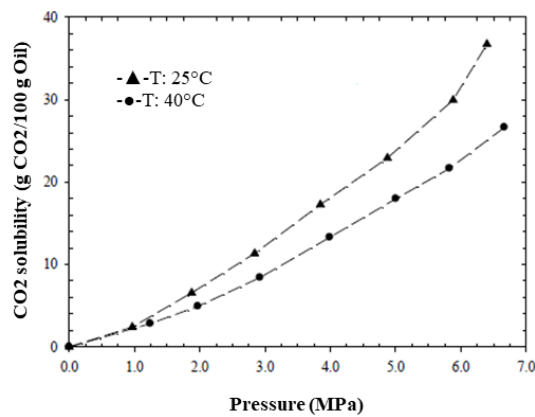


Fig. 5. CO₂ solubility in light crude oil as a function of pressure [12]

The topic of oil solubility in supercritical CO₂ has also been investigated in the literature. The solubility of non-polar hydrocarbons in supercritical CO₂ is significantly higher than that in gaseous CO₂. The enhanced solubility is attributed to the liquid-like density of the supercritical CO₂ which promotes strong attractive forces. Decreasing the supercritical fluid density through expansion to subcritical pressure or a relatively small increase in temperature leads to a reduction in supercritical CO₂ dissolving power as well as separation of the extract and CO₂.

The *n*-alkanes solubility in supercritical CO₂ at 318 – 343k and pressures up to 32 MPa was measured in a fixed volume, high-pressure-view chamber with the aim of obtaining a correlation between CO₂ density and *n*-alkanes solubility in supercritical CO₂ [36]. The hydrocarbon content of the high-pressure cell was stirred to attain the setpoint temperature. Once the setpoint temperature was reached, CO₂ was injected into the cell until a clear transparent single phase was formed. After equilibration, the system was gradually depressurized by letting out some CO₂ until precipitation of the solute out of the single-phase

solution was visually detected, which results in cloudiness of the mixture in the high-pressure cell (Fig. 6). System pressure at this point is the cloud point pressure of the solvent (i.e., CO₂) and the solubility is calculated as follow:

$$x(\%) = \frac{(m_1/M_1)}{[m_1/M_1 + (v_0\rho_0)/M_0]} \times 100 \quad (1)$$

where, x is the mole fraction of the solute, m_1 is the mass of the solute, v_0 is the cell volume, ρ_0 is the density of CO₂, and M_1 and M_0 are the molecular weights of solute and CO₂, respectively.

The solubility of *n*-alkanes (S in kg/m³) can then be obtained as follow:

$$S = \frac{\rho M_1 x}{[M_0(1-x)]} \quad (2)$$

It was shown that hydrocarbon solubility has direct impact on CO₂ density. Furthermore, an increase in pressure is accompanied with an increase in the *n*-alkanes solubility in supercritical CO₂, while their solubility has inverse relation with temperature and chain length [36].

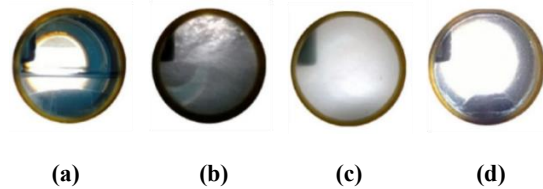
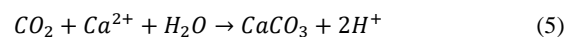
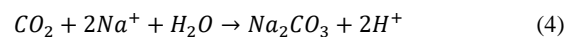


Fig. 6. Solubility of *n*-hexane in supercritical CO₂ at 45°C and a) P=5.445 MPa, b) P=5.445 MPa under stirring, c) P=7.712 MPa under stirring, and d) P=8.630 MPa under stirring [36]

3 CO₂ interactions with rock minerals

CO₂, in all forms of gas, liquid, dissolved in water or supercritical can react with cations in the formation water, leading to precipitation of carbonate minerals, which is illustrated in the form of reactions 3 to 5 below [2, 6]. This conversion of CO₂ to carbonate minerals, also known as mineral trapping mechanism, is considered as the safest storage mechanism with minimized leakage likelihood [37]. However, carbonate mineral precipitation could potentially lead to some flow assurance issues if other conditions for agglomeration and deposition are met, which ultimately may adversely impact the reservoir quality for carbon storage.

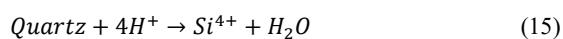
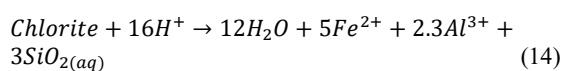
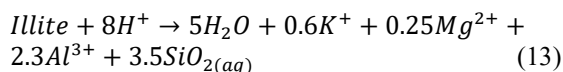
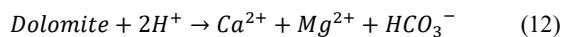
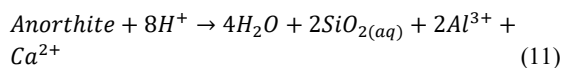
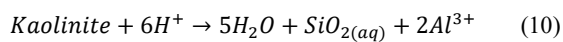


Another important aspect of CO₂ injection into geological formations is the dissolution of CO₂ in

the aqueous phase which leads to the formation of weak carbonic acid (reaction 6). Carbonic acid has two acidic hydrogens and two dissociation constants (reactions 7 and 8) [38, 39].



The dissociation of carbonic acid initiates a series of reactions with *in-situ* fluids and formation rocks depending on temperature, pressure, flow regime, fluid composition, and mineralogy of the rock. Some of these reactions may be beneficial to the CO₂ storage (i.e., increased accessible pore space, enhanced surface injectivity through increased permeability, and enhanced storage through mineral trapping) while others may adversely impact the CO₂ storage (i.e., impaired permeability due to inorganic deposition facilitated with mineral re-precipitation, formation of CO₂ migration pathways, and caprock failure) [16, 38, 40-42]. Due to the dissociation of carbonic acid, an acidic solution with the pH of 3.4 is formed upon dissolution of CO₂. The formation minerals are susceptible to carbonic acid. They may be dissolved and eventually leach out [5]. This mineral dissolution, particularly for the case of caprock minerals, is crucial to understand in order to examine caprock integrity to address CO₂ leakage issues. The minerals can react with acid under very different dissolution rates. The extent of CO₂-brine-rock interactions is governed by the dominant state of carbonic acid with respect to pH [16]. The reactions that occur depend on the mineral composition and are affected by temperature, pressure, flow regime, brine composition, multiphase flow of CO₂ and water, and initial pore structure [40, 43, 44]. Carbonate minerals such as calcite, dolomite, magnesite, and some magnesium-carbonate minerals tend to precipitate (reactions 9-15), while clay minerals dissolve [2, 5, 40, 42, 45].



The reactions of carbonates and other minerals with CO₂-saturated brine leads to the consumption

of protons and increase of the brine pH. Therefore, metal ions are released to the solution. At high concentration of metal ions, the increase in pH can lead to reprecipitation of some minerals. The precipitation or reprecipitation of minerals within the shale matrix may lead to “self-sealing of fractures” and “caprock strengthening” [44, 46-49]. The effects of mineral dissolution and re-precipitation on the pore system and permeability of shale have not been well described in the literature.

4 CO₂-brine systems and the pH

Understanding *in-situ* brine chemistry is important when injecting foreign fluids (i.e., chemicals, carbon dioxide, a secondary brine phase etc.) into the geological formations. This is necessary for investigating the kinetics of mineral dissolution, designing optimal salinity and pH windows for chemical injections, as well as studying the compatibility between the *in-situ* and injecting fluids [50]. The *in-situ* brine pH is a critical parameter, and knowledge of the dynamic pH changes at high-pressure conditions in geological carbon storage is essential for proper interpretation of the reactive transport phenomena and associated geochemical reactions. However, real *in-situ* measurements of pH under high pressure conditions during CO₂ injection into saline aquifers or depleted oil reservoirs have not been studied extensively in the literature. Considering several chemical and geochemical reactions occurring between the injected CO₂, *in-situ* brine, injected brine (if carbonated water is being injected), rock minerals and *in-situ* oil, knowledge of the pH variations provides insights into the extent, type and rate of these reactions. It also helps to diagnose some other phenomena associated with these reactions. For instance, dissolution of CO₂ in brine results in production of carbonic acid and pH reduction, which also reduces the crude oil emulsion(s) stability [51]. On the contrary, when the CO₂-saturated brine reacts with carbonates and other minerals, protons are being consumed which results in pH increase.

Typically, the solution pH in CO₂-brine systems is estimated through calculation based on solubility of CO₂ in the aqueous phase using Henry’s law and the known first and second dissociation constants of carbonic acid at the corresponding temperature, pressure, and electrolyte composition. Geochemical simulators such as PHREEQC and EQ3NR are being used for calculating pH values at high temperatures and pressures [16, 38, 52, 53]. However, these pH predictions become difficult in high ionic-strength solutions, and limited experiments have been conducted to validate the results of such simulations for the CO₂-brine systems. In addition, there are discrepancies between simulations and experimental results [54].

Two common methods used for measuring pH in CO₂-brine systems under reservoir conditions are electrometric and optical [55, 56]. Optical methods, such as UV-vis spectrophotometry, are rapid, simple, and precise. In this technique, the pH is measured through observing the spectra of a pH sensitive dye (i.e., bromophenol blue). However, they have not been extensively applied for CO₂-brine systems at HPHT conditions due to the need for introduction of an indicator to the system which may not be stable under these extreme operating conditions.

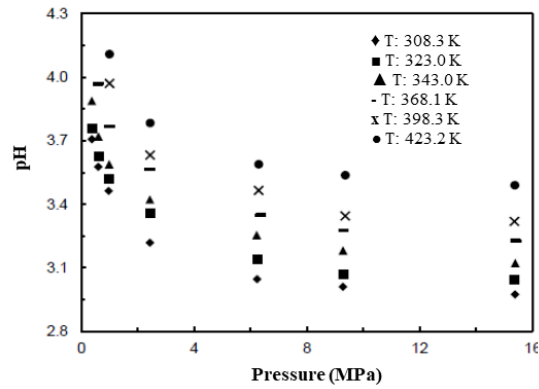
A common practice for measuring pH has been to collect brine samples from the effluent of coreflooding setup or the batch reactor containing CO₂-rock-brine mixture. A pH-sensitive glass electrode, a reference electrode, and a meter are then used to measure pH of the degassed brine samples. However, this type of fluid analysis does not represent real *in-situ* test conditions because pH variations as a result of pressure and ionization equilibrium reactions will not be captured. Peng et al. conducted a study using an electrometric technique to investigate how pH is affected by temperature, pressure, and CO₂ solubility in water [9]. This study is relevant to CO₂ sequestration in deep formations with temperature and pressure ranges up to 423 K and 15 MPa, respectively. It was found that the reference electrode (Ag/AgCl) was vulnerable to sudden pressure drops, leading to leakage in the system. The solution pH was found to have a direct relation with temperature (Fig. 7(b)) and CO₂ content (Fig. 8), but an inverse relation with pressure (Fig. 7(b)).

Different solid-state metal oxides, especially iridium oxide film electrodes, have been found superior in performance compared to the conventional glass electrodes due to their long lifespan, mechanical stability, corrosion resistance, fast response, and high sensitivity [50, 57, 58]. The effectiveness of iridium oxide-based chemical sensors for *in-situ* pH measurement of the produced water samples under HPHT and high-salinity conditions was evaluated in the literature, and the measurements were found to be highly accurate and also not disturbed by the high pressure condition. These sensors seem to be a promising tool for pH measurement in such harsh operating conditions of high pressure, temperature and salinity. As an example, Yu et al. [50] studied the performance of an iridium oxide-based chemical sensor for *in-situ* measurement of pH of produced water samples under high pressure (up to 3000 psi), high temperature (up to 80°C), and high salinity condition. Despite the presence of interfering ions (i.e., Na⁺, Mg²⁺, Cl⁻, SO₄²⁻), the iridium oxide pH sensor proved to be highly sensitive and showed a slight positive shift in pH potential when sodium chloride was present.

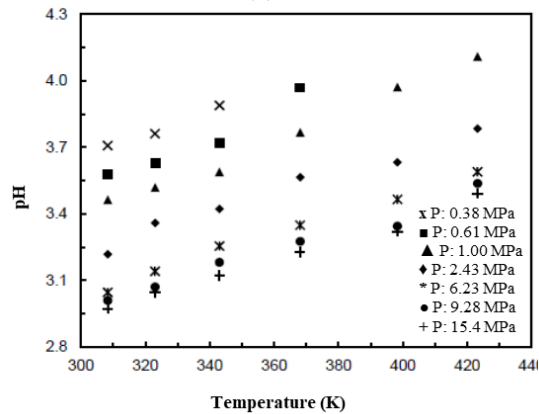
5 Experimental studies of CO₂ storage in geological formations

Understanding the multiphase flow in porous media at the pore-level is crucial in evaluating the long-term destiny of the CO₂ being injected into a geological formation. This understanding is essential in comprehending the underlying physics at the macroscopic scale. The formation heterogeneity, characterized by porosity, permeability and capillary pressure distributions complicates the process of CO₂ dissolution [59, 60]. Therefore, detailed knowledge of the geological architecture and permeability is necessary. Several mechanisms contribute to CO₂ storage in saline aquifers, including structural trapping, residual trapping, solubility trapping, and mineral trapping, and their interaction is intricate, time-dependent, and heavily influenced by local conditions [3, 5-7]. This complexity highlights the need for a comprehensive understanding of the mechanisms involved.

Structural trapping occurs when the injected CO₂ is trapped below an impermeable caprock due to the buoyancy effect. Residual trapping occurs when the injected CO₂ flows through the rock pores and displaces the *in-situ* fluids, leaving behind small trapped droplets of CO₂ due to capillary forces. Solubility trapping occurs over a longer period of time, where a portion of the injected CO₂ is dissolved into the formation brine at the pore-level, which is greatly dependent on various factors such as salinity, pH, temperature, and geological structures. Lastly, mineral trapping happens when the formation brine, containing dissolved CO₂, reacts with rock minerals. There are several important parameters affecting CO₂ mineral trapping including temperature, pressure, salinity, rock mineral composition, aquifer thickness and anisotropy, and the number of aquifer layers [7, 19].



(a)



(b)

Fig. 7. pH of the CO₂-water system as a function of pressure (a) and temperature (b) [9]

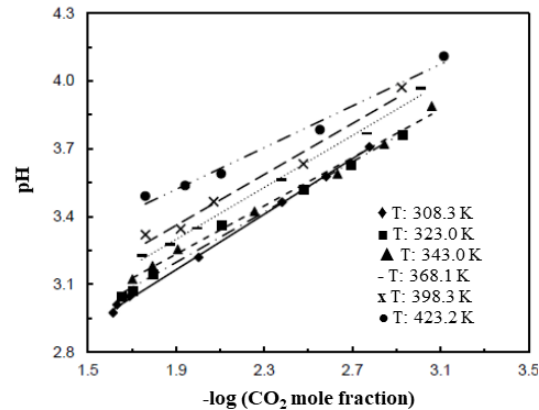


Fig. 8. pH of the CO₂-water system as a function of CO₂ mole fraction [9]

For the case of CO₂ storage in saline aquifers, experimental studies and theoretical calculations are needed to comprehend the chemical interactions between the CO₂ and brine-saturated rock samples. Several lab-scale coreflooding experiments have been conducted to simulate CO₂ injection and migration processes in deep saline aquifers. A partial list of these experimental case studies is provided in Table 1, along with information on rock/fluid properties, operating conditions, and measurement techniques associated with each reference. These experiments were all performed

Table 1: Some selected laboratory studies on CO₂ geological sequestration in saline aquifers

under *in-situ* HPHT conditions. The porous media prototypes used in these studies include synthetic or real core plugs, stacked core assemblies, or packed beds of glass beads. Various analytical techniques were used for rock and fluid characterization, as well as quantification and visualization of rock-fluid interactions for the CO₂-brine multiphase migration through the porous structures.

Rock mineralogy plays a crucial role in the long-term success of CO₂ geological storage due to the variety and extent of the chemical and geochemical reactions between the injected CO₂, native fluid(s) in place, and rock minerals. Rosenhauer et al. [38] conducted experiments to study reactions between CO₂ and natural and synthetic brines in the presence of limestone and sandstones. They found that the reaction of CO₂-saturated low-sulfate brine with limestone dissolved 10% of calcite and increased porosity by 2.6%, while the porosity decreased by 4.5% in the presence of high sulfate brine. They also observed that CO₂ solubility in brine was enhanced by 6% and 5% in the presence of limestone and arkosic sandstone, respectively. Various analytical techniques including coulometric titration, inductively coupled plasma – atomic emission spectroscopy (ICP-AES), ion chromatography (IC), and potentiometric titration were used to measure the concentration of dissolved species and pH.

Lin et al. studied the physicochemical interactions in the supercritical CO₂-water-rock (i.e., quartz, biotite, and granite) systems using a hydrothermal autoclave cell at 100°C [61]. The hydrothermal effects on the primary minerals and the occurrence of any secondary minerals were evaluated using scanning electron microscopy (SEM) and energy dispersive X-ray analysis (EDX). Four reaction systems were considered in this study: supercritical CO₂-rock without water, water-rock without CO₂ (i.e., the control sample), supercritical CO₂-saturated steam-rock, and CO₂-water-rock. When water was not present in the system, no distinct chemical alterations were observed in the supercritical CO₂-rock system. Furthermore, the elemental concentrations in the supercritical CO₂-biotite system with water were significantly greater than that in the water-biotite system, which highlights the impact of supercritical CO₂ on the chemical alterations.

Shi et al. conducted a study to determine the CO₂ residual saturation and understand how CO₂ is trapped in the saline aquifers [62]. They injected supercritical CO₂ and CO₂-saturated brine into a Berea sandstone core at 10 MPa and 40°C and used an X-ray CT scanner to map changes in the fluid saturation and porosity throughout the core. The results were then simulated using a 1D model, where air-water capillary pressure data were used in the absence of relative permeability data as a first approximation for the CO₂-brine system.

CO ₂ physical state	Rock type	Initial Porosity and Permeability	Fluids	Analytical and Characterization Methods	Ref.
scCO ₂	Siltstone caprock (35% quartz, 53% kaolinite, 8% muscovite, 3% alunite, 1% other minerals)	Porosity: 7.65% Permeability: 0.23 μD	Synthetic brine (NaCl, CaCl ₂ , KCl, MgCl ₂) dissolved in deionized water	X-ray diffraction (XRD) and SEM were used to analyze the mineralogical composition and morphology of the core samples, respectively. Porosity was evaluated with CT scanning and saturation methods. ICP-OES was used for analysis of the brine samples.	[42]
scCO ₂	Shale (Quartz, K-feldspar, Albite, Calcite, Dolomite, Pyrite, Clay).	Porosity: ~5% Permeability: ~0.2 μD	Synthetic brine (NaCl, CaCl ₂ , KCl, MgCl ₂)	The ions concentrations in brine before and after each static soaking test were measured with ICP-AES. SEM, XRD, EDS were used to characterize mineralogical, pore structure, and mechanical properties of the core samples.	[16]
scCO ₂	Berea sandstone	Permeability: 914 mD	Brine	Water and CO ₂ were injected into the core samples in a loop of fluids recirculation from outlet to the inlet. Steady-state relative permeability tests were performed to determine CO ₂ /water relative permeability-saturation relationship.	[73]
gCO ₂ , scCO ₂	Carbonate aquifer (CaCO ₃)	Porosity: 0.3-26.8% Permeability: 2.9-451.9 mD	NaBr brine	Porosity and permeability measurements were conducted with x-ray CT scanning.	[43]
CO ₂ dissolved in brine	Shale	-	CO ₂ -saturated brine	3D micro-CT scanning of core samples from a shale gas reservoir was performed before and after 5 hours of CO ₂ -saturated brine injection (flow rate: 0.1 mL/min).	[74]
Liquid CO ₂ , scCO ₂	Sandstone	Porosity: 18% Brine permeability: 2.74-45.71 mD	3 wt% brine (NaCl, KCl, CaCl ₂ , MgCl ₂ , MgSO ₄)	Relative permeability to brine was first measured by injecting brine into each vacuumed core at constant flow rate and then Darcy equation was used to calculate the absolute permeability for each core. CO ₂ (liquid or supercritical) was injected into the core samples at 0.3564 g/min.	[75]
scCO ₂	Arqov and Berea Sandstone	Berea porosity and permeability: 19.5-19.9% and 276 mD	CO ₂ /Water	X-ray CT scanning and mercury injection capillary pressure (MICP) were used for porosity and saturation measurement.	[76]
CO ₂ dissolved in water	Berea sandstone	Porosity: 20.5%	Water	X-ray CT scanning was used to measure CO ₂ saturation and to observe its spatial distribution.	[77]
gCO ₂ , scCO ₂	Sandstone	Porosity: 27% Permeability: 1.14 D	Brine, gCO ₂ -saturated brine, scCO ₂ -saturated brine	Mineralogical analysis was performed by XRD, and the rock sample morphology was evaluated with SEM.	[65]
Liquid CO ₂	Sandstone (Quartz, Feldspar, Dolomite, and Clay)	porosity: 15.8% Initial water permeability: 85 mD	Deionized water	Magnetic resonance imaging (proton NMR) was used for two-phase CO ₂ /water flow characterization in a coreflooding set up. The mineralogical composition was assessed through XRD.	[10]

In a field-scale trial of geological carbon sequestration, Pang et al. studied CO₂ injection into a depleted oil reservoir [63]. The post-injection gas and water samples were periodically collected from the monitoring wells. Upon analyzing the gas samples, their methane and CO₂ contents were found at 86.7 - 95.1% and 0.1 - 1.6%, respectively. It is reported that the brine samples were not affected by CO₂ injection during the monitoring period even though the analytical method that resulted in this conclusion is not specified in the paper. The latter conclusion was reached focusing on the bicarbonate ion concentration in the water samples, which first gradually decreased during the first day of CO₂ injection but then plateaued for the rest of the monitoring period. The reason was hypothesized to be related to the CO₂-saturated brine not reaching the monitoring wells during the monitoring period.

Rathnaweera et al. conducted a study on the interactions between supercritical CO₂, brine and sandstone rock samples for over 1.5 years of exposure time at 10 MPa and 40°C [64]. They found that long-term exposure to CO₂ caused a significant decrease in pH as well as dissolution of minerals such as calcite, siderite, barite, and quartz. This created a drying-out effect and precipitation of salt, which altered the mineralogical structure and permeability of the rock sample(s). The team performed high-pressure tri-axial permeability measurement tests on the reacted rock samples and used SEM analysis to identify mineralogical changes. It was found that changes in the pore structure affected the effective stress response of the rock samples. The elemental composition of the virgin brine samples was also analyzed using ICP-MS and ICP-AES methods, but no analysis was reported on the reacted brine samples after completion of the high-pressure permeability tests.

During fracturing of shale reservoirs with HPHT supercritical CO₂ as the fracturing fluid, the reactions between CO₂, brine and rock samples occur rapidly, and stronger reactions are likely to occur in the carbonate-rich shales with higher porosity and permeability [16]. Furthermore, successful CO₂ injection and storage requires geological formations with adequate permeability and porosity values, and carbonate-rich sandstones are therefore, the preferred host rocks [16, 64].

Jayasekara et al. conducted chemical analyses on brine-saturated siltstone to study the geochemical equilibrium between the formation fluid and caprock in order to assess potential caprock integrity failure [42]. They found that the siltstone permeability to supercritical CO₂ was significantly decreased at high salinities due to the CO₂ dry-out effect, which resulted in deposition of water evaporates and evaporites in the pore space. It was also found that the pH of CO₂-

saturated brine, in contact with the rock sample, was significantly decreased; however, it is not mentioned whether the pH decrease was experimentally measured or predicted using a software package. As a conclusion drawn from this study, aquifers that contain higher salinity *in-situ* brine are more appropriate candidates for CO₂ storage because over geological time exposure of their caprock to the high-salinity brine, significant reductions in its porosity and permeability has had occurred, resulting in greater caprock integrity when long-term storage of CO₂ is concerned.

To evaluate changes in the topology of minerals and elemental composition of sandstone core samples for CO₂ sequestration, microscopic image analysis was used [65]. The samples were reported to be homogeneous with an average porosity of 27%, obtained using saturation method, and permeability of 1.14 Darcy. According to the XRD mineralogical analysis, the samples were mostly composed of 79.5 wt.% quartz and 4.34 wt.% kaolinite. This elemental composition was changed due to the CO₂-brine-rock interactions. The presence of brine accelerated these changes. Furthermore, the porosity of samples reduced after saturation with supercritical CO₂ (scCO₂)-brine and gaseous CO₂-brine fluids due to precipitation of clays that clogged the pores. This porosity reduction was more pronounced in the samples saturated with scCO₂-brine fluid.

During CO₂-EOR process, CO₂ can be trapped at the pore-scale through capillary and solubility trapping; the two mechanisms that are mainly controlled by pore structure and wettability [66]. Various studies have investigated the effects of wettability and heterogeneity on 2-phase oil-water flow dynamics [67, 68]. However, the trapping mechanisms are more complex when a gaseous and/or supercritical phase CO₂ is involved, where two conflicting views have been reported in the literature. On one hand, it is believed that the CO₂ trapping efficiency increases when the pore system becomes more water-wet [66]. The other perspective states that the CO₂ trapping efficiency increases when the pore surface becomes less water-wet [69, 70].

Li et al. used CT images to study the effects of pore geometry and wettability on the 3-phase flow involving CO₂, oil and water under immiscible conditions. Their findings indicate that strong heterogeneity and water-wet conditions are more favorable for CO₂ trapping [71]. In a water-wet system, CO₂ was trapped as gas-in-water, whereas in an oil-wet system, CO₂ was directly surrounded by oil and occupies the pore space originally filled by oil and water. These experiments were carried out at atmospheric pressure and room temperature to avoid miscibility. However, CO₂ is found in supercritical or

liquid form under reservoir conditions, and there is a need to study the 3-phase behaviour for these CO₂ physical states.

Several studies have examined how the distribution of fluids in porous media is affected by sub-core heterogeneity, and how this affects the ability of formations to sequester CO₂ through residual trapping mechanism. For instance, Kou et al. [72] conducted tests on two types of core samples with different permeability levels to study how the sub-core heterogeneity affects the behaviour of supercritical CO₂-brine mixtures. They used nuclear magnetic resonance (NMR) measurements at both the core and sub-core scales and found that ignoring the sub-core scale heterogeneity can lead to significant uncertainties in predicting storage and fluid flow displacement during the CO₂ injection.

6 Conclusions

In this article, we discussed the potential of CO₂ storage in geological formations as a solution method to mitigate global warming. Saline aquifers and depleted oil and gas reservoirs are the preferred reservoirs due to their large storage capacity. Injection of CO₂ into these formations requires a detailed understanding of multiphase flow behaviour, fluid-fluid and fluid-rock interactions. The article presented a review of experimental studies on the CO₂ phase behaviour associated with CO₂ storage in geological formations and its interactions with formation brine, remaining oil in place, and formation rock. Changes in capillary pressure and relative permeability properties due to the CO₂-induced interactions requires more quantification efforts and site-specific reservoir data, and its comprehensive review could be the subject of a separate review article. During CO₂ injection, multiphase equilibrium can be encountered and there is a need for building thermodynamic models and robust algorithms for such systems. pH changes can affect the stability of clay and carbonate minerals, and dissolution, transport, and re-precipitation of carbonate could occur when CO₂ is being injected into a carbonate reservoir. Therefore, a better understanding of the physicochemical properties of CO₂-brine systems, especially in the presence of porous media, is essential to advance the field of geological carbon storage and improve the sustainability of energy industry.

Acknowledgments

The authors would like to thank the Hibernia Management and Development Company (HMDC),

Chevron Canada Ltd, Energy Research and Innovation Newfoundland and Labrador (ERINL), the Natural Sciences and Engineering Research Council of Canada (NSERC), the Province of Newfoundland and Labrador, and Mitacs for financial support.

References

1. R. Shukla, P. Ranjith, A. Haque, X. Choi, *Fuel*, **89**, 2651 (2010)
2. P. Kelemen, S.M. Benson, H. Pilorgé, P. Psarras, J. Wilcox, *Front. Clim.*, **1**, 9 (2019)
3. C.M. White, B.R. Strazisar, E.J. Granite, J.S. Hoffman, H.W. Pennline, *J. Air Waste Manag. Assoc.*, **53**, 645 (2003)
4. D.Y.C. Leung, G. Caramanna, G., M.M. Maroto-Valer, M. M., *Renew. Sust. Energ. Rev.*, **39**, 426 (2014)
5. Y. Fang, B. Baojun, T. Dazhen, S. Dunn-Norman, D. Wronkiewicz, *Pet. Sci.*, **7**, 83 (2010)
6. T. Ajayi, J.S. Gomes, A. Bera, *Pet. Sci.*, **16**, 1028 (2019)
7. S. Kumar, J. Foroozesh, K. Edlmann, M.G. Rezk, C.Y. Lim, *J. Nat. Gas Sci. Eng.*, **81**, 103437 (2020)
8. H.T. Schaef, B.P. McGrail, *Greenhouse Gas Control Technologies*, **2**, 2169 (2005)
9. C. Peng, J.P. Crawshaw, G.C. Maitland, J.P.M. Trusler, D. Vega-Maza, *J. Supercrit. Fluids*, **82**, 129 (2013)
10. J.C. Manceau, J. Ma, R. Li, P. Audigane, P.X. Jiang, R.N. Xu, J. Tremosa, C. Lerouge, *Water Resour. Res.*, **51**, 2885 (2015)
11. T. Suekane, S. Soukawa, S. Iwatani, S. Tsushima, S. Hirai, *Energy*, **30**, 2370 (2005)
12. N. Mosavat, F. Torabi, *Energy Procedia*, **63**, 5408 (2014)
13. L.I. Eide, M. Batum, T. Dixon, Z. Elamin, A. Graue, S. Hagen, S. Hovorka, B. Nazarian, P.H. Nøkleby, G.I. Olsen, P. Ringrose, R.A.M. Vieira, *Energies*, **12**, 1945 (2019)
14. A. Witkowski, M. Majkut, S. Rulik, *Arch. Thermodyn.*, **35**, 117 (2014)
15. P.S. Ringrose, A.K. Furre, S.M.V. Gilfillan, S. Krevor, M. Landro, R. Leslie, T. Meckel, B. Nazarian, A. Zahid, *Annu. Rev. Chem. Biomol. Eng.*, **12**, 471 (2021)
16. Y.S. Zou, S.H. Li, X.F. Ma, S.C. Zhang, N. Li, M. Chen, *Int. J. Greenh. Gas Con.*, **49**, 157 (2018)
17. Z. Chen, Y. Zhou, H. Li, *Ind. Eng. Chem. Res.*, **61**, 10298 (2022)
18. Y. Peysson, L. Andre, M. Azaroual, *Int. J. Greenh. Gas Con.*, **22**, 291 (2014)
19. G.P.D. De Silva, P.G. Ranjith, M.S.A. Perera, *Fuel*, **155**, 128 (2015)

20. Z. Duan, R. Sun, 2003. *Chem. Geol.*, **193**, 257 (2003)
21. F. Tabasinejad, R.G. Moore, S.A. Mehta, K.C. Van Fraassen, Y. Barzin, *Ind. Eng. Chem. Res.*, **50**, 4029 (2011)
22. S. Kim, Y. Kim, B.H. Park, J.H., J.W. Kang, *Fluid Phase Equilib.*, **328**, 9 (2012)
23. A. Chapoy, M. Nazeri, M. Kapateh, R. Burgass, C. Coquelet, B. Tohidi, *Int. J. Greenh. Gas Con.*, **19**, 92 (2013)
24. G. Comak, S. Foltran, J. Ke, E. Perez, Y. Sanchez-Vicente, M.W. George, M. Poliakoff, *J. Chem. Thermodyn.*, **93**, 386 (2016)
25. Z. Wang, Q. Zhou, H. Guo, P. Yang, W. Lu, *Fluid Ph. Equilibria.*, **476**, 170 (2018)
26. T.J. Behbahani, C. Ghotbi, V. Taghikhani, A. Shahrabadi, *Energy & Fuels*, **26**, 5080 (2012)
27. P. Zanganeh, S. Ayatollahi, A. Alamdari, A. Zolghadr, H. Dashti, S. Kord, *Energy & Fuels*, **26**, 1412 (2012)
28. B. Ju, T. Fan, Z. Jiang, *J. Pet. Sci. Eng.*, 109, 144 (2013)
29. A.A. Gabrienko, O.N. Martyanov, S.G. Kazarian, *Energy & Fuels*, **30**, 4750 (2016)
30. D. Yang, P. Tontiwachwuthikul, Y. Gu, *J. Chem. Eng. Data*, **50**, 1242 (2005)
31. A. Georgiadis, G. Maitland, J.P.M. Trusler, A. Bismarck, *J. Chem. Eng. Data*, **55**, 4168 (2010)
32. R.W. Klusman, *Energy Convers. Manag.*, **44**, 1921 (2003)
33. L. Chiamonte, M. Zoback, J. Friedmann, V. Stamp, C. Zahm, *Energy Procedia*, **4**, 3973 (2011)
34. M. Godec, V. Kuuskraa, T. Van Leeuwen, L.S. Melzer, N. Wildgust, *Energy Procedia*, **4**, 2162 (2011)
35. J. Lv, Y. Chi, C. Zhao, Y. Zhang, H. Mu, *R. Soc. Open Sci.*, **6**, 181902 (2019)
36. Q. Shi, L. Jing, W. Qiao, *J. CO₂ Util.*, **9**, 29 (2015)
37. S. Zhang, D.J. DePaolo, *Acc. Chem. Res.* **50**, 2075 (2017)
38. R.J. Rosenhauer, T. Koksalan, J.L. Palandri, *Fuel Process. Technol.*, **86**, 1581 (2005)
39. S. Hurter, D. Labregere, J. Berge, *SPE 108540* (2007)
40. G. Cui, Y. Wang, Z. Rui, B. Chen, S. Ren, L. Zhang, *Energy*, **155**, 281 (2018)
41. G. Cui, L. Zhang, C. Tan, S. Ren, Y. Zhuang, C. Enechukwu, *J. CO₂ Util.*, **20**, 113 (2017)
42. D.W. Jayasekara, P.G. Ranjith, W.A.M. Wanniarachchi, T.D. Rathnaweera, A. Chaudhuri, *A. Energy*, **191**, 116486 (2020)
43. O. Izgec, B. Demiral., H. Bertin, S. Akin, *SPE-94697* (2005)
44. R. Chang, S. Kim, S. Lee, S. Choi, M. Kim, Y. Park, *Front. Energy Res.*, 5, 1 (2017)
45. O. Ozotta, M. Ostadhassan, K. Liu, B. Liu, O. Kolawole, F. Hadavimoghaddam, *J. Pet. Sci. Eng.*, **206**, 109071 (2021)
46. C.A. Rochelle, I. Czernichowski-Lauriol, A.E. Milodowski, *Geol. Soc. Spec. Publ.*, **233**, 87 (2004)
47. M. Calabrese, F. Masserano, M.J. Blunt, *SPE 95820* (2005)
48. A. Busch, P. Bertier, Y. Gensterblum, G. Rother, C.J. Spiers, M. Zhang, H.M. Wentinck, *Geomech. Geophys. Geo.*, **2**, 111 (2016)
49. J. Rohmer, A. Pluymakers, F. Renard, *Earth-Sci. Rev.*, **157**, 86 (2016)
50. J. Yu, M. Khalil, N. Liu, R. Lee, *Ionics*, **21**, 855 (2015)
51. G. Sun, D. Liu, C. Li, D. Yang, G. Wei, F. Yang, B. Yao, *Energy & Fuels*, **32**, 9330 (2018)
52. I. Ceyhan, A. Santra, A.S. Cullick, *SPE 141031* (2011)
53. M. Garcia-Rios, J. Cama, L. Luquot, J.M. Soler, *Chem. Geol.*, **383**, 107 (2014)
54. D.E. Allen, B.R. Strazisar, Y. Soong, S.W. Hedges, *Fuel Process. Technol.*, **86**, 1569 (2005)
55. R.K. Haghi, A. Chapoy, L.M.C. Peirera, J. Yang, B. Tohidi, *Int. J. Greenh. Gas Con.*, **66**, 190 (2017)
56. J.D. Müller, B. Schneider, S. Abmann, G. Rehder, *Limnol. Oceanogr. Meth.*, **16**, 68 (2018)
57. R.H. Zhang, X.T. Zhang, S.M. Hu, *Anal. Chem.*, **80**, 2982 (2008)
58. L. Manjakkal, D. Szwagierczak, R. Dahiya, *Prog. Mater. Sci.*, **109**, 100635 (2020)
59. R. Farajzadeh, P. Ranganathan, P.L.J. Zitha, J. Bruining, *Adv. Water Resour.*, **34**, 327 (2011)
60. M. Iding, M.J. Blunt, *Energy Procedia*, **4**, 4961 (2011)
61. H. Lin, T. Fujii, R. Takisawa, T. Takahashi, T. Hashida, *J. Mater. Sci.*, **43**, 2307 (2008)
62. J.Q. Shi, Z. Xue, S. Durucan, *Energy Procedia*, **4**, 5001 (2011)
63. Z. Pang, Y. Kong, Y. Li, J. Li, *Procedia Earth Planet. Sci.*, **7**, 656 (2013)
64. T.D. Rathnaweera, P.G. Ranjith, M.S.A. Perera, *Sci. Rep.*, **6**, 19362 (2016)
65. A. Peter, X. Jin, X. Fan, K.I.-I.I. Eshiet, Y. Sheng, D. Yang, *J. Pet. Sci. Eng.*, **208**, 109411 (2022)
66. K. Chaudhary, M.B. Cardenas, W.W. Wolfe, J.A. Maisano, R.A. Ketchum, P.C. Bennett, *Geophys. Res. Lett.*, **40**, 3878 (2013)
67. S. Bakhshian, H.S. Rabbani, S.A. Hosseini, N. Shokri, *Geophys. Res. Lett.*, **47**, 1 (2020)
68. F.G. Wolf, D.N. Siebert, R. Surmas, *Phys. Fluids*, **32**, 052008 (2020)
69. R. Holtzman, E. Segre, *Phys. Rev. Lett.*, **115**, 164501 (2015)

70. K. Singh, H. Scholl, M. Brinkmann, M. Di Michiel, M. Scheel, S. Herminghaus, R. Seemann, *Sci Rep*, **7**, 1 (2017)
71. Y. Li, Y. Yang, M. Dong, J. Yao, K. Zhang, H. Sun, L. Zhang, *SPE 212830* (2022)
72. Z. Kou, H. Wang, V. Alvarado, J.F. McLaughlin, S.A. Quillinan, *J. Hydrol.*, **599**, 126481 (2021)
73. 41. S. Krevor, R. Pini, L. Zuo, S.M. Benson, *Water Resour. Res.*, **48**, 1 (2012)
74. H. Yu, Y. Zhang, M. Lebedev, Z. Wang, J. Ma, Z. Cui, M. Verrall, A. Squelch, S. Iglauer, *Energy Procedia*, **154**, 125 (2018)
75. P. Tawiah, H. Wang, S.L. Bryant, M. Dong, S. Larter, J. Duer, *Int. J. Greenh. Gas Con.*, **112**, 103491 (2021)
76. R. Pini, S. Krevor, S.M. Benson, *Adv. Water Resour.*, **38**, 48 (2012)
77. J.C. Perrin, R.W. Falta, S. Krevor, L. Zuo, K. Ellison, S.M. Benson, *Energy Procedia*, **4**, 3210 (2011)